energies

MDPI

Article

Feasibility Study and Economic Analysis of a Fuel-Cell-Based CHP System for a Comprehensive Sports Center with an Indoor Swimming Pool

Jie Liu, Sung-Chul Kim and Ki-Yeol Shin *

School of Mechanical Engineering, Yeungnam University, 280 Daehak-ro, Gyeongsan-si 712-749, Korea; lauj@ynu.ac.kr (J.L.); sungkim@ynu.ac.kr (S.-C.K.)
* Correspondence: shinky@ynu.ac.kr; Tel.: +82-53-810-3060

Abstract: Unlike a general commercial building, heating for a building with an indoor swimming pool is highly energy-intensive due to the high energy demand for swimming water heating. In Korea, the conventional heating method for this kind of building is to use boilers and heat storage tanks that have high fuel costs and greenhouse gas emissions. In this study, a combined heat and power (CHP) system for such a building using the electricity and waste heat from a Phosphoric Acid Fuel Cell (PAFC) system was designed and analyzed in terms of its primary energy saving, CO_2 reduction, fuel cell and CHP efficiency, and economic feasibility. The mathematical model of the thermal load evaluation was used with the 3D multi-zone building model in TRNSYS 18 software (Thermal Energy System Specialists, LLC, Madison, WI, USA) to determine the space heating demand and swimming pool heat losses. The energy efficiency of the fuel cell unit was evaluated as a function of the part-load ratio from the operating data. The fundamental components, such as the auxiliary boiler, thermal storage tank, and heat exchanger are also integrated for the simulation of the system's operation. The result shows that the system has a high potential to improve the utilization efficiency of fuel cell energy production. Referring to the local condition of the energy market in Korea, an economic analysis was also carried out by using a specific FC-CHP capacity at 440 kW. The economic benefit is significant in comparison with a conventional heating system, especially for the full-time operating (FTO) mode. The net profit made by comparison with the conventional energy supply system is about 178,352 to 273,879 USD per year, and the payback period is expected to be 6.9 to 10.7 years under different market conditions.

Keywords: fuel cell (FC); phosphoric acid fuel cell (PAFC); combined heat and power (CHP); wasted heat recovery system (WHRS); strategic energy management planning; economic analysis

Citation: Liu, J.; Kim, S.-C.; Shin, K.-Y. Feasibility Study and Economic Analysis of a Fuel-Cell-Based CHP System for a Comprehensive Sports Center with an Indoor Swimming Pool. *Energies* **2021**, *14*, 6625. https://doi.org/10.3390/en14206625

Academic Editors: Jan Danielewicz and Krzysztof Rajski

Received: 31 August 2021
Accepted: 10 October 2021
Published: 14 October 2021

1. Introduction

The main motivations to seek more clean and efficient methods of energy production are the increasing cost of fuel and the need for the reduction of CO_2 and harmful emissions [1]. A combined heat and power (CHP) system has many benefits when it is used to provide electrical and thermal energy for commercial buildings, such as increasing power reliability; the reduction of primary energy consumption, greenhouse gas emissions and costs; and the improvement of power quality [2]. Furthermore, the owner of the CHP system can benefit from the higher efficiency of the fuel energy conversion, the lower cost of fuel per unit of energy, high-quality power, and the rapid variation of the distribution between electrical and thermal loads [3]. For the application of commercial buildings, CHP is decentralized electrical power generation coupled with thermally activated components [4]. In the CHP part, the interest in the improvements of the primary generator over a typical thermal engine to new is growing more, especially in Japan, and more recently in Europe [5]. Comparing with those other CHP technologies, such as Stirling engines or gas turbines, fuel cells—as an electrochemical generator—can achieve substantially higher

efficiencies and potentially compete even the most energy-efficient large-scale power plants in terms of electric efficiencies [6,7], due to their wide range of capacities which can be well matched with the energy demand, thereby increasing the energy utilization.

According to the electrolyte and operating temperature, fuel cells can be categorized into the following five major types: alkaline fuel cells (AFC), proton exchange membrane fuel cells (PEMFC), solid oxide fuel cells (SOFC), phosphoric acid fuel cells (PAFC), and molten carbonate fuel cells (MCFC). A comparison of the characteristics of different types of fuel cells is listed in Table 1 [8]. Referring to the features of different types of fuel cells, several studies about fuel-cell-based CHP systems were carried out. In Ivan Verhaert et al.'s study, an AFC based micro-CHP system was compared with other micro-CHP technologies, and it was shown that for buildings with a decreasing heating demand and increasing electricity demand, a fuel-cell-based micro-CHP has a better result, especially, in terms of thermal performance [9]. PEMFC has a major application in transportation due to its potential impact on the environment, such as the control of greenhouse gases emissions [10]. However, due to its high efficiency and low pollution in comparison with conventional combustion-based power generation technologies, PEMFC is also considered to be a prospective alternative power source for distributed energy or CHP applications [11]. A thermodynamic analysis for a combined cooling, heating, and power (CCHP) system based on PEMFC as a prime mover has been performed, and the results indicated that the energy and exergy efficiencies of the CCHP system are 81.55% and 54.5% [12]. SOFC has several advantages, such as high electrical efficiency, high-quality heat supply, small installation footprints, the flexibility of its fuel use, and the use of economical materials [13]; it has successfully been verified in long-term stationary power generation up to the Megawatt-scale, generally for the use of commercial CHP systems. A 175 kW SOFC-CHP system was analyzed, and it successfully decreased annual utility costs by up to 14.5% over a baseline HVAC system [14]. Techno-economic analyses of a PEMFC- and SOFC-based micro-CHP system for a residential application with [15] and without a heat pump [16] were carried out by Marta Gandiglio et al., and the results indicate that a SOFC–CHP system has a better total energy efficiency (up to 81%), and the PEMFC-CHP system presents a total efficiency of 75% and a 3-year payback period. PAFC has a relatively low operating temperature, low-electrolyte cost, and high durability in comparison with the other types of fuel cell technologies. Therefore, the PAFC is believed to be one of the most complete fuel cell technologies, and is easy to commercialize [17,18]. As early as 10 years ago, it was demonstrated that the PAFC has high reliability, efficiency, and flexibility for a variety of applications, especially for distributed power generation [19]. Compared with SOFC, the PAFC cannot be effectively used to drive a heat engine due to its relatively low working temperature. However, the operating temperature of PAFC is higher than PEMFC, and the waste heat recovered from PAFC includes a considerable amount of available energy [20]. The economic and environmental potential of a CHP system based on a 400 kW scale PAFC was introduced by a simulation-based analysis under two different operation strategies, and the results indicated that the electrical load following (ELF) model would be the advisable operation mode for this CHP system in the residential sector [21]. Salvador Acha et al. investigated the feasibility of a 460 kW PAFC-based CHP system in the application of a commercial building. The results indicated that the FC-CHP system is financially competitive against the internal combustion engine [22].

Table 1. Comparison of fuel cell technologies.

	AFC	MCFC	PEMFC	PAFC	SOFC
Operating temperature	60–90 °C	600–700 °C	<120 °C	150–200 °C	500–1000 °C
Electrical efficiency	45–60%	45–60%	45–60%	40%	60%
Typical capacity	<100 kW	300 kW–3 MW	<1–100 kW	5–440 kW	1 kW–2 MW
Applications	Military; Backup power;	Electric utility; Distributed generation;	Distributed generation; Transportation; Specialty vehicles;	Distributed generation; CHP;	Electric utility; Distributed generation;

From the above literature, for the analysis of the operating and economic performance of a fuel-cell-based CHP system, relatively accurate load data plays a vital role, as the CHP performance is highly dependent on the load matching condition. The analysis without complete annual load data [12,13] can just present the performance of the CHP system under specific operating conditions, but is limited to reflect the fluctuation of the load, which has the biggest impact on the performance of the CHP system. Some of the studies used measured data or standard profiles of electricity and thermal loads [5,15,16,21]. It is effective for the analysis of existing building or if the building has a relatively standard load profile according to their functions, such as a school, office, commercial buildings, etc. However, for buildings that are under construction and have a special load profile, such as a commercial building with an indoor swimming pool, the better way is to obtain the load through numerical simulation. The commercial software eQUEST [14] and EnergyPlus [23] were found to be used for the thermal load evaluation for the analysis of a fuel-cell-based CHP system. However, the effective verification of the simulation results of the load was not found. Therefore, in order to overcome the aforementioned limitations, a weather-data-based dynamic computation model for the fuel-cell-based CHP system, which includes the thermal load evaluation of a comprehensive sports center with an indoor swimming pool is developed in this study, and the obtained thermal load is validated by the measured data from a reference building.

The comprehensive sports center with an indoor swimming pool is planned and under construction in Donghae City, Gangwon Province, South Korea. Unlike general commercial buildings, a building with an indoor swimming pool is highly intensive in the use of thermal energy, due to the high heat loss from the pool water. The conventional strategy of energy supply for this kind of building is to provide electrical energy from the main grid and thermal energy from a combustion boiler. Normally, for a general commercial building in Korea, the thermal–electrical load ratio is around 0.5 [24]. However, for a building with an indoor swimming pool, it could be larger than 0.7. This characteristic will improve the utilization rate of waste heat from the fuel cell. The thermal–electrical ratio of the PAFC output is from 0.7 to 1.2 under different part-load conditions which are closer to the aimed-for building than the SOFC (0.5). Moreover, by considering its lower temperature of operating and waste heat, the PAFC is the better choice for the design building than SOFC, although the SOFC has a higher electrical efficiency. In this study, two operating strategies of the FC-CHP system are introduced and analyzed from the following aspects: primary energy consumption, fuel cell and CHP efficiency, and economic feasibility. In the aspect of the energy load, the measured data of the electricity load from a similar building is modified and used. The thermal energy demand, including the heating load, swimming pool heat loss, and domestic hot water demand, is evaluated by the commercial software TRNSYS, which is also used for the dynamic simulation of the system's operation. Figure 1 depicts the main configuration of the designed FC-CHP system for the building. In the PAFC system, the fuel cell stack produces both electrical and thermal energy from the hydrogen produced through the reforming of natural gas. The main electrical and thermal load are provided by fuel cell production. Simultaneously, the electricity from the main power grid and the heat from an auxiliary boiler are also required as a supplement. The performance of a CHP system is highly dependent on the operating strategies due to the unstable characteristics of the load over time. From the perspective of exergy efficiency, there are two representative regimes of operating strategies: electrical load tracking (ELT) and thermal load tracking (TLT) [23,25]. However, from the economic point of view, more electricity production means more revenue, especially in a country with an open electricity market, because the excess electricity production could be sold onto the grid. The TLT model presents a significant shortage in the total amount of power generation in the summer season. Therefore, the TLC model is not considered to be an operating strategy. Additionally, the operating strategy of so-called full time operating (FTO) is carried out in this study. This operating model is always applied in a large scale fuel cell plant [26,27], but is not common in CHP applications. The performance and economic feasibility should

be analyzed and compared with the ELT model and traditional energy supply method. In these regards, the main objectives of this study are as follows:

- The evaluation of the thermal loads—which includes the space heating load, swimming pool loss, and hot water demand—by developing a weather-data-based dynamic simulation model, and validation using reference data.
- The evaluation of the performance of the 440 kW PAFC-based CHP system in terms of primary energy saving, system efficiency, and CO_2 reduction with ELT and FTO models.
- The economic feasibility of the 440 kW PAFC-based CHP system in the aspects of net profit (NP) and payback period (PP) under different market conditions.

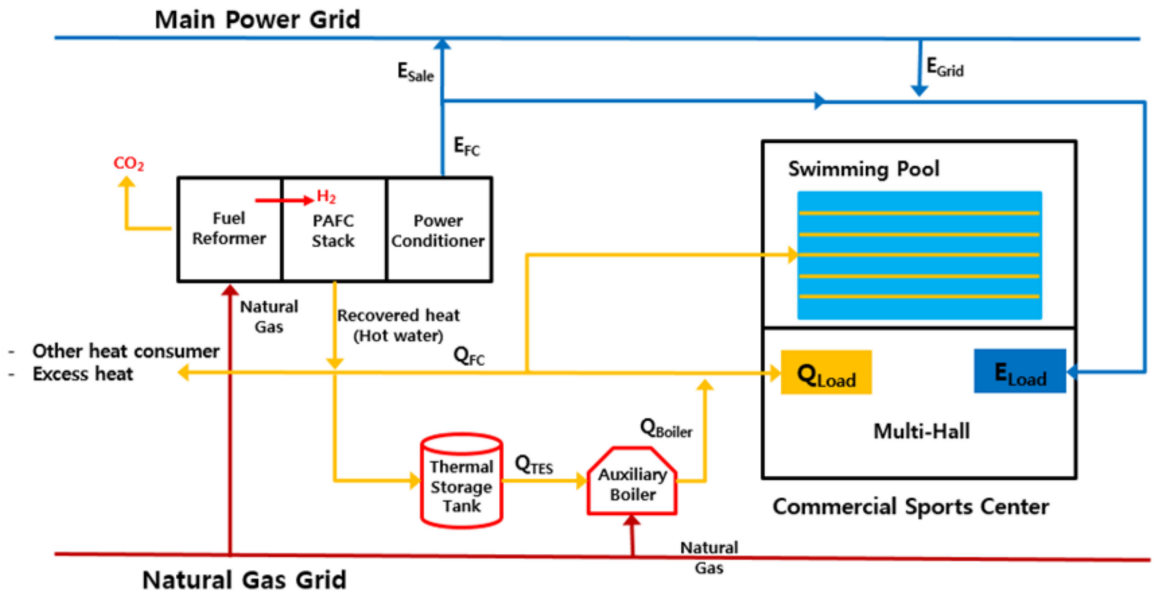

Figure 1. Configuration of the designed FC-CHP system.

2. Model Approach

Figure 2 describes the operating strategies of the designed FC-CHP system. For the ELT model, the fuel cell will operate following the building electricity demand. The power from the main city grid will be a supplement when the building electricity load is less than the minimum capacity (100 kW) or larger than the maximum capacity of the fuel cell (440 kW). In the meantime, the fuel cell's waste heat will be recovered and supply the building thermal energy demand directly, or will be re-stored in a thermal storage tank. When the fuel cell waste heat supply is insufficient, the heat in the heat storage tank will be released to meet the heating demand. When the system is operating under the FLO model, both the power and heat are the maximum generated. Unlike the ELT model, much more excess power is generated and could be sold onto the main power grid. An auxiliary boiler is used for some extreme conditions under both of the two operating models. The dynamic simulation results of the above two operating strategies of the FC-CHP system will be compared with the conventional energy supply strategy.

The dynamic simulation of the FC-CHP system based on the measured electricity load, evaluated thermal load, and fuel cell performance data was also produced in the TRNSYS software. Figure 3 presents the configuration of the model in the TRNSYS simulation studio. The components are modeled by parameters, inputs, and outputs, and are linked with each other by following the operating strategy. The parameters of the main components in the system are introduced in Table 2.

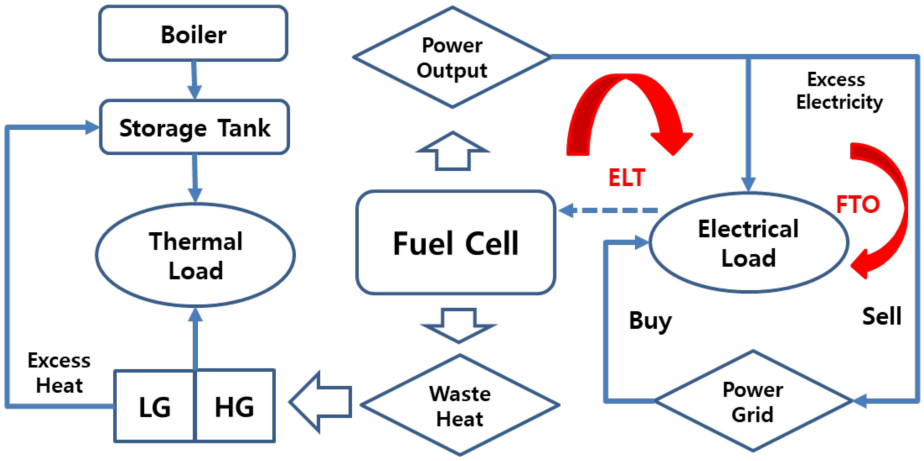

Figure 2. Operating strategy of FC-CHP system.

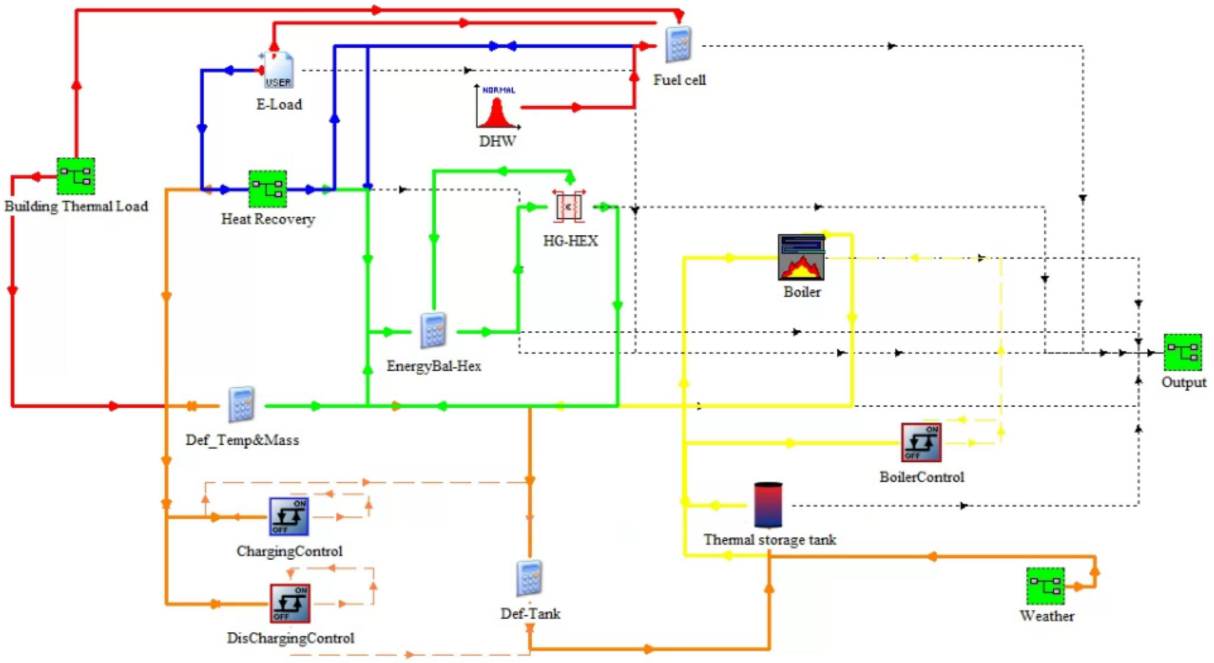

Figure 3. Interface of the fuel-cell-based CHP system simulation in the TRNSYS software.

Table 2. Parameters of the main components used in the system simulation.

Components	Parameters	Values
Fuel cell	Rated electrical capacity, kW	440
	Electrical efficiency, 100%	0.24–0.45
	Thermal efficiency, 100%	0.27–0.49
	Wasted water temperature, °C	60, 121
Heat exchanger	Efficiency, 100%	0.85
Thermal storage tank	Size, m^3	50
Auxiliary boiler	Rated capacity, kW	100

2.1. Performance Data of the PAFC

The performance data of the PAFC—which can present the correlations between the fuel cell's operating part load and the power output, waste heat recovery, and the fuel energy consumption—was obtained from the fuel cell manufacturer [28], and is described in Figure 4. The PAFC can provide the maximum power of 440 kW, and was suggested

to operate with a turndown ratio of 0.227, which means the PAFC will not operate at less than 22.7% (about 100 kW) of its rated power. The recovered waste heat can be supplied to the thermal load of the building at two levels of water temperature: high-grade (HG, about 120 °C), and low-grade (LG, about 60 °C). Among them, the LG heat can be recovered over all of the operating time, and the HG heat can be recovered only when the part-load is larger than 51.1%. The electrical power efficiency and thermal efficiency of the fuel cell system are defined as:

$$\eta_{E-FC} = E_{FC}/F_{FC} \quad (1)$$

$$\eta_{Q-FC} = Q_{FC}/F_{FC} \quad (2)$$

where E_{FC} is the electric power produced by the fuel cell unit, Q_{FC} is the total recovered thermal energy, and F_{FC} is the fuel (natural gas) energy consumption of the fuel cell. Thus, the overall efficiency of the fuel cell system is given as:

$$\eta_{FC} = \eta_{E-FC} + \eta_{Q-FC} \quad (3)$$

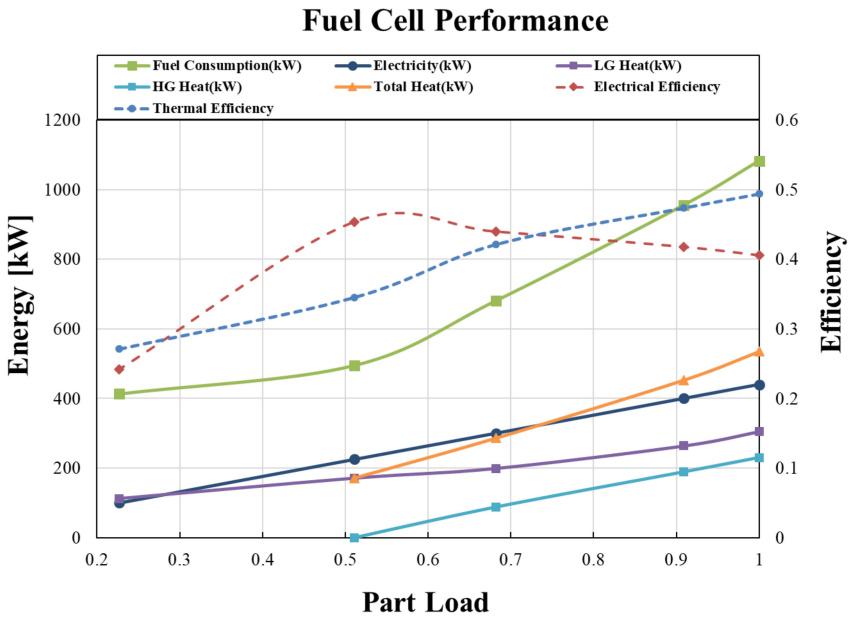

Figure 4. Correlation performance data for a 440 kW PAFC.

For the FTO model, it is suggested that the fuel cell is operated with the maximum power output all the time, even when the electrical power efficiency is not the highest. As shown in Figure 4, the $\eta_{E\text{-}FC}$, $\eta_{Q\text{-}FC}$ and η_{FC} of the suggested PAFC with the maximum electrical power output reach 40.6%, 49.4%, and 90%, respectively. For the approached ELT model, the fuel cell energy production and efficiency will be calculated with the correlations by responding to the building energy load.

2.2. Electricity Load

In this study, a comprehensive sports center with an indoor swimming pool, which is under construction in Donghae City, Korea, is planned to use a 440 kW PAFC-based CHP system for its electrical and thermal energy supply. We first investigated the measured hourly electricity load of a referenced commercial building which has a similar location, construction, floor area, building function, and activity schedule for one year as the input data for the dynamic simulation. As shown in Figure 5a, high electricity demand is present in the summer season due to the large cooling energy which is consumed by the electric air conditioner, and after sorting the hourly load in descending order, it can be seen that there are about 2400 h of electricity demand in a year, which is higher than the maximum capacity of the fuel cell (440 kW), and thus requires auxiliary supply from the main power

grid if the fuel cell is operating with the FTO model. If the fuel cell is working with the ELT model, there is still about 3800 h of electricity demand that requires assistance from the main power grid, when the electricity load is lower than the minimum capacity of the fuel cell (100 kW). From a general calculation, about 4.18% and 13.28% electricity demand is required from the main power grid when the fuel cell is working with the FTO and ELT model respectively. The detailed electricity load distribution for the first week in January shown in Figure 5b presents a significant load profile of a commercial building. The measured data reflects the seasonal and daily characteristics of the electrical load well, and will be used as the input data for the dynamic system simulation.

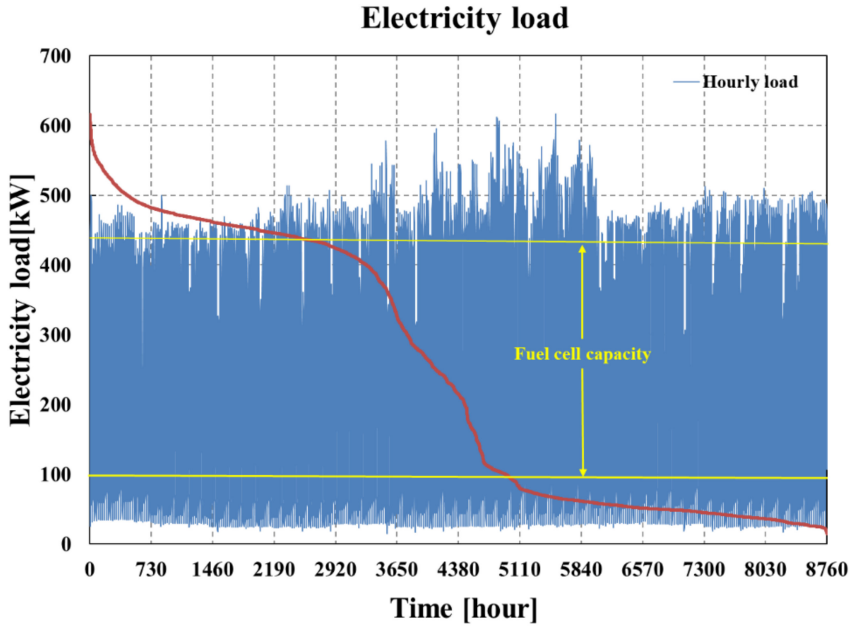

(**a**)

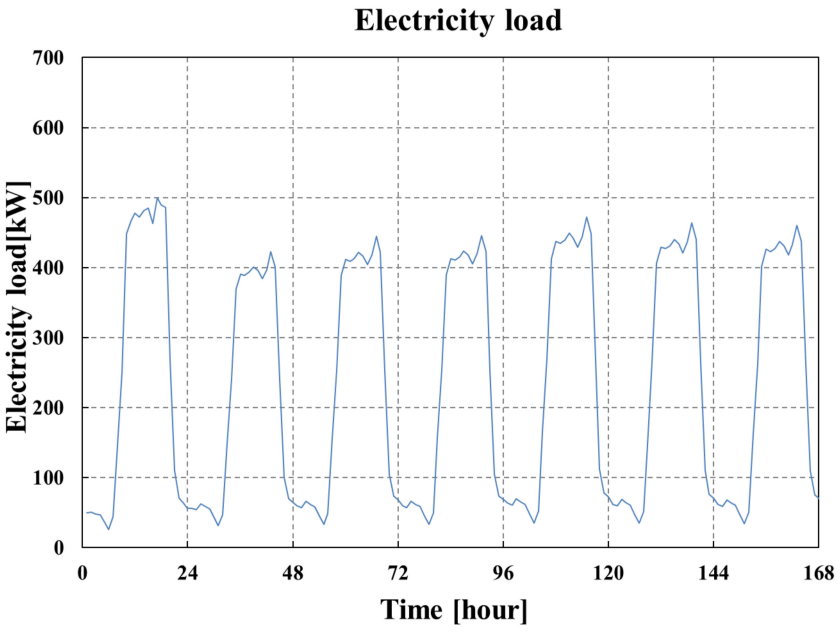

(**b**)

Figure 5. Measured electricity load ((**a**) annual; (**b**) weekly).

2.3. Thermal Load Evaluation

The thermal energy demand of the building is composed of three parts: space heating, swimming pool heat loss, and domestic hot water. A general method to investigate the thermal energy load is to account for the fuel consumption. However, in this study, it is difficult to obtain completed data on fuel consumption, especially in hours. Therefore, in this study, the commercial software TRNSYS—which has been approved by several researchers—is used to evaluate the thermal energy demand.

The 3D building model in TRNSYS is used for the space heating thermal load evaluation. The building geometry was first modelled using Google SketchUp, see Figure 6, then the material properties of the envelope were incorporated in TRNBuild, a 3D building-modelling program integrated into TRNSYS. After that, the weather data (ambient temperature, solar radiation, wind speed, soil temperature, etc.) were input to the TRNBuild component, and the hourly space heating load was calculated in TRNSYS Simulation Studio. The detailed configuration of thermal load macro that was integrated in the CHP system model is shown in Figure 7.

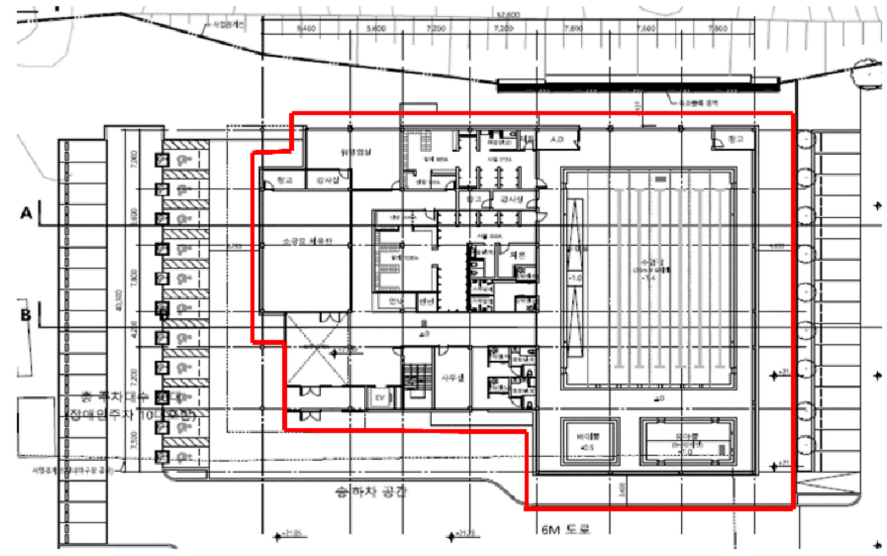

(**a**)

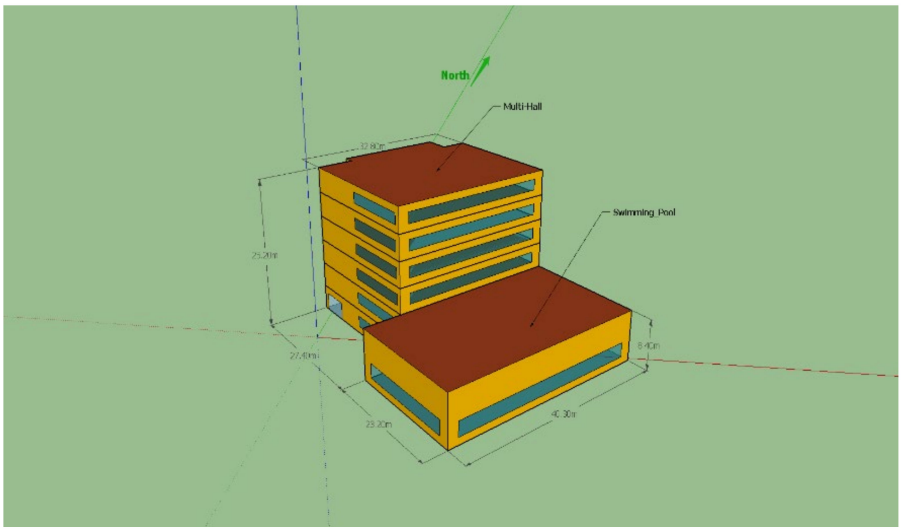

(**b**)

Figure 6. An architectural plan of the comprehensive sports center with an indoor swimming pool (**a**) and the 3D modeling (**b**).

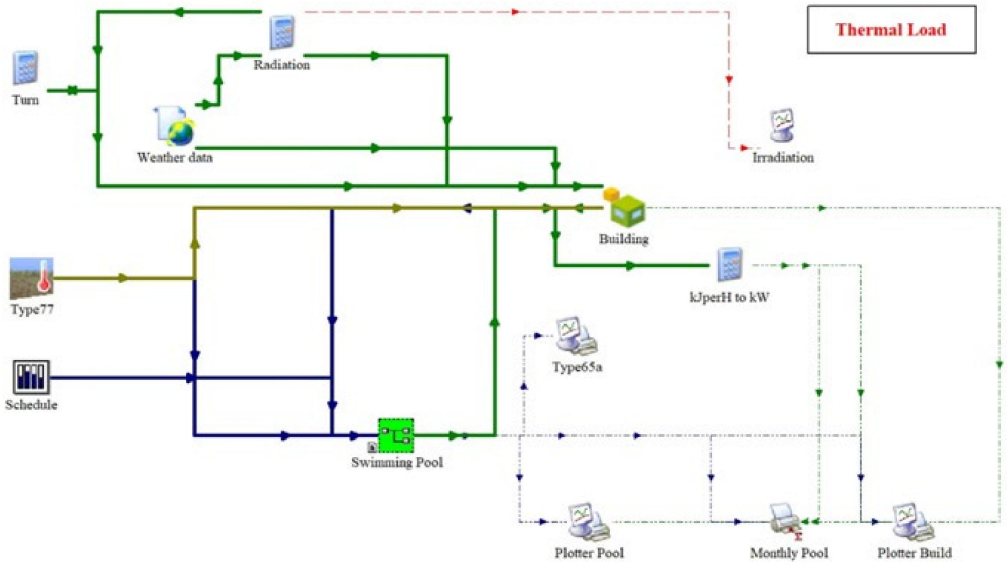

Figure 7. Interface of the building thermal load simulation macro in the TRNSYS software.

The evaluation of the heat loss of the indoor swimming pool is generally based on Thomas Auer's model [29] and is integrated into the TRNSYS thermal load model. The heat loss of the swimming pool Q_{loss} includes four parts:

$$Q_{loss} = Q_{evp} + Q_{conv} + Q_{cond} + Q_{rad} \tag{4}$$

where Q_{evp} is the heat loss by evaporation from the swimming pool surface, which can be calculated by:

$$Q_{evp} = m_{evp} h_{evp} \tag{5}$$

where h_{evp} is the evaporation heat of the water at setting temperature (kJ/kg, 2439.3 kJ/kg for 26 °C water), and m_{evp} is the amount of evaporation water (kg/m^{2}h), which can be calculated by [30]:

$$m_{evp} = A_s(4.08 + 4.28v)(x_{sa,m} - x_a) \tag{6}$$

where $x_{sa,m}$ and x_a are the maximum humidity ratio of saturated air at the same temperature as the water surface (kg/kg, 26 °C is 0.0212858 kg/kg) and the humidity ratio of ambient air (kg/kg, setting in TRNSYS). A_S is the surface area of the swimming pool.

The convection heat loss of swimming pool water Q_{conv} can be calculated on the basis of Newton's formula:

$$Q_{conv} = hA_s(T_{sw} - T_{air}) \tag{7}$$

where T_{sw} and T_{air} are the temperatures of the swimming pool water and the indoor air, respectively. The convective heat transfer coefficient (W/m^2 °C) can be expressed as a linear function of the indoor air speed v, as follows [31]:

$$h = 2.8 + 3.0v \tag{8}$$

Due to the poor heat conductance of soil, the conductive heat loss through the side walls and bottom of the swimming pool is relatively small, and can be calculated by:

$$Q_{cond} = UA_{pw}(T_{sw} - T_{pw}) \tag{9}$$

where the A_{pw} is the wall and bottom area of the swimming pool. U is the conductive heat transfer coefficient (W/m^2 °C).

The heat transfer by long-wave radiation with the wall surfaces of the hall can be calculated on the basis of the Stefan–Boltzmann law (Equation (10)). For an indoor swimming pool, the pool area can be assumed to be completely enclosed.

$$Q_{rad} = \sigma \varepsilon A_s (T_{sw}^4 - T_{cel}^4) \quad (10)$$

where σ is the Stefan–Boltzmann constant (5.67×10^{-8} W/m^2 °C^4), and ε is the emissivity of the swimming pool water surface (0.9 in this study).

The domestic hot water is mainly consumed by the showering of the customers, and is given as normally distributed random values with a mean value of 25 kW in the simulation; the parameters for the TRNSYS simulation are listed in Table 3.

Table 3. Building and swimming pool parameters.

Components	Parameter with Units	Values
Building	Total floor area, m^2	7418.96
	Wall u-value, W/m^{2}K	0.651
	Window u-value, W/m^{2}K	1.1
	Window g-value, 100%	0.62
	Ground u-value, W/m ^{2}K	0.295
	Indoor setting temperature, °C	25
	Indoor humidity ratio, 100%	0.5–0.7
Swimming pool	Surface area, m^2	25 × 15
	Deepth, m	1.5
	Wall heat transfer coefficient, W/m^{2}K	0.25

3. Simulation Results

Thermal load validation is always required to validate a simulation result against measured data. In our case, due to the objective building being under plan, we collected the thermal energy consumption of the building which used to provide the electricity load. It is necessary to mention that unlike the electricity load, it is very difficult to obtain a complete fuel consumption, especially in hours. The daily fuel consumption data for the referenced commercial building is only available for the month of January 2020. The heat supply to the building is from a gas boiler with an average efficiency of 0.85 [32]. The loss from the delivery system is assumed to be 10%. The error indicators used in this study are the MBE (Mean Bias Error) and CV-RMSE (Coefficient of Variance of the Root Mean Square Error), defined as [33]:

$$\mathrm{MBE} = \frac{\sum \left(\mathrm{Measured}_{\mathrm{day}} - \mathrm{TRNSYS}_{\mathrm{day}}\right)}{\sum \left(\mathrm{Measured}_{\mathrm{day}}\right)} \times 100\% \quad (11)$$

$$\mathrm{CV-RMSE} = \frac{\mathrm{RMSE}_{\mathrm{day}}}{\mathrm{Mean}\left(\mathrm{Measured}_{\mathrm{day}}\right)} \times 100\% \quad (12)$$

$$\mathrm{RMSE} = \sqrt{\frac{\sum \left(\mathrm{Measured}_{\mathrm{day}} - \mathrm{TRNSYS}_{\mathrm{day}}\right)^2}{(\mathrm{Numberofday}) - 1}} \quad (13)$$

Figure 8 compares the daily heating load predicted by TRNSYS with the measured data. Due to the missing measured data for the 1st, 23th, and 24th, the simulation result for these 3 days was also removed for the validation. After the processing, the MBE was within the acceptable range (less than 5%), but the CV-RMSE was above the criteria for a calibrated model (less than 15%). In consideration that the measured data was only evaluated from the normal record of boiler fuel consumption, not a strict experiment, we can say this is an acceptable error, and the thermal load evaluated by TRNSYS can be used in the dynamic simulation of the FC-CHP system. Figure 9 presents the results of the evaluation of the

space heating load and swimming pool heat loss based on the weather data of Donghae city. The peak load values are about 330 kW and 120 kW for space heating and swimming pool heat loss. For the swimming pool, high heat loss is also presented even in summer, due to the evaporation heat loss accounting for the largest proportion of the total heat loss.

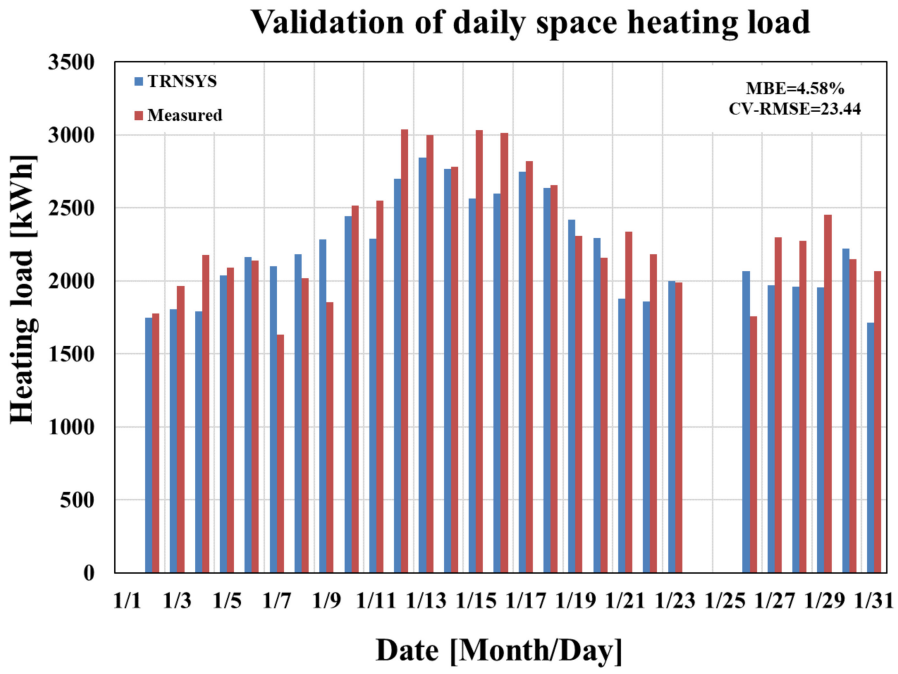

Figure 8. Validation of the daily heating energy consumption between the simulation data and measured data.

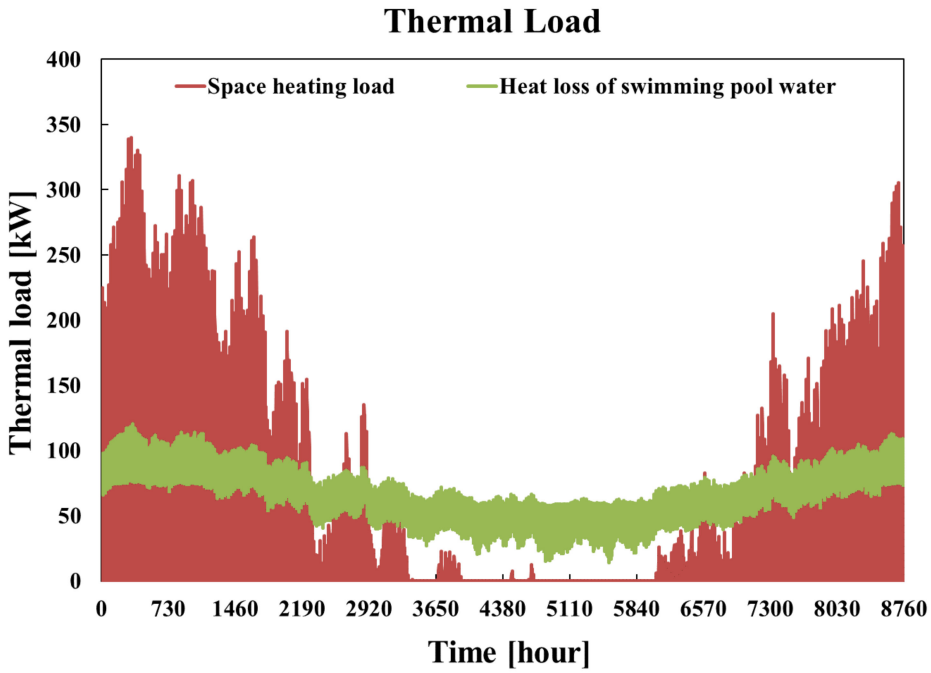

Figure 9. Building space heating load and swimming pool heat loss evaluated by the TRNSYS simulation.

Figure 10 presents the simulation results of the energy demand and supply of the FC-CHP system with the ELT (a) and FTO (b) FC operating strategy, including the building electricity load, thermal load, fuel cell electric power generation, heat generation (high grade and low grade), and effective heat. For the ELT model, the fuel cell will not work during the night time due to the electricity load being less than 100 kW, which is the

minimum electric power capacity of the fuel cell. For the FTO model, the fuel cell is working at the maximum capacity all of the time, so that both the electric power and thermal heat generation are presented as the constant maximum value. Here, it has to be mentioned that, for the thermal heat supply for a commercial building, the high-grade waste heat from a fuel cell that has a temperature of about 120 °C cannot be supplied to the building directly. A heat exchanger is recommended to transform the high-grade heat temperature to a low grade. Therefore, considering the heat exchanger efficiency, the effective heat is necessary to evaluate and be used for the analysis of the primary energy saving and economic feasibility.

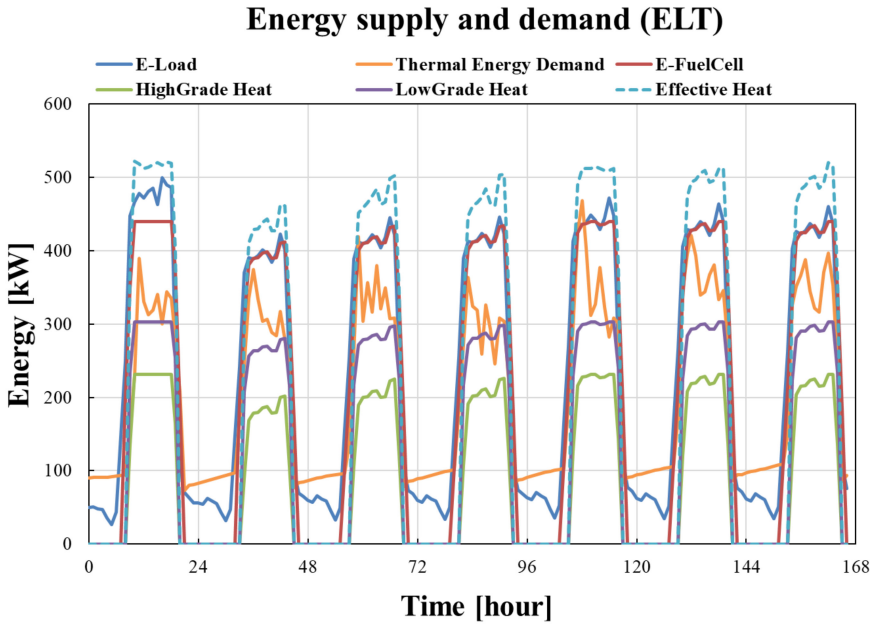

(**a**)

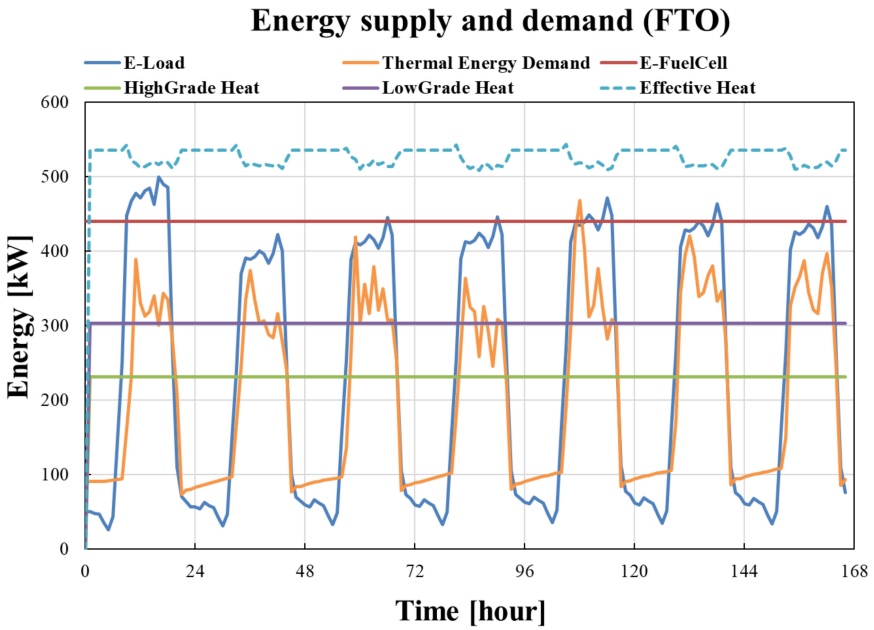

(**b**)

Figure 10. Energy demand and supply of FC-CHP systems for the first week of January ((**a**) ELT model; (**b**) FTO model).

The primary energy consumption for both the ELT and FTO models are evaluated from the annual system simulation. The results are compared with a reference case with a conventional power and heat supply method. The primary energy consumption can be evaluated as:

$$PEC = F_{FC} + F_b + F_{GE} \quad (14)$$

where F_{FC}, F_b, and F_{GE} are the fuel energy consumption of the fuel cell, boiler, and electric power supplied from the main power grid. For the FC-CHP system, the fuel cell and boiler fuel energy consumption can be evaluated from the simulation directly. In the case of the conventional energy supply method, the efficiency of the gas boiler and grid power are assumed to be 0.85 [32] and 0.35 [34,35], respectively.

Figure 11 presents the monthly primary energy consumption in the case of the ELT and FTO models in the FC-CHP system, and the conventional energy supply. The ELT model has lower primary energy consumption than the other two cases, and compared with the reference case, it can save about 10% to 15% fuel energy in the winter season. During the summer, even the large heat loss of the swimming pool can be covered by the fuel cell waste heat; the energy saving is not obvious due to the fact that the fuel cell is always operated with a relatively low efficiency under the ELT model. The FTO model consumes much more fuel energy than the two other cases due to its longer working time and high electrical output capacity. However, from a macro point of view, the FTO model still has its own advantages, such as high electrical efficiency and high waste heat generation.

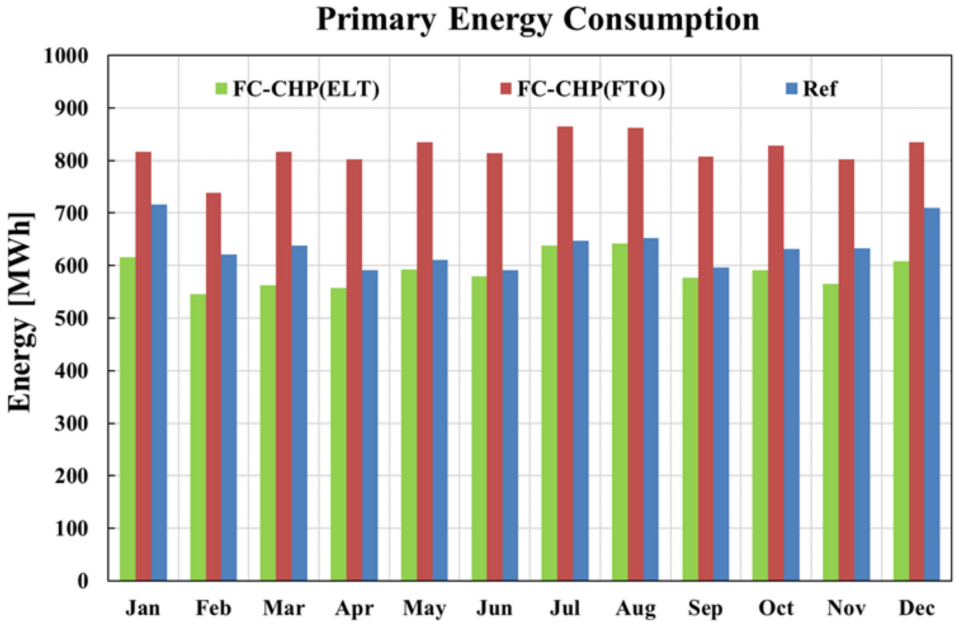

Figure 11. Primary energy consumption for the three case studies (ELT and FTO models in FC-CHP systems and the conventional energy supply model).

The CHP system can play an important role in both the primary energy saving and the reduction of CO_2 emissions. The evaluation of CO_2 emissions is complex due to its being highly dependent on the type of primary energy source. For the fuel cell system used in this study, from the manufacturer's report, the CO_2 emission factor is 0.453 tCO_2/MWh [28]. The CO_2 emission factors of coal and natural gas are assumed to 0.9 and 0.4 tCO_2/MWh, respectively [36]. For the natural gas boiler, the emission factor is set to be 0.2 tCO2/MWh. Therefore, by considering the fraction of electricity generation by the source types, the CO_2 emissions can be evaluated. As can be seen from Figure 12, whether the CHP system is operating in the ELT model or FTO model, the CO_2 emissions of the system are significantly lower than the traditional energy supply mode. Even the FTO model has a large primary energy consumption; the CO_2 emissions are still much lower than the conventional energy system due to the high fuel cell efficiency.

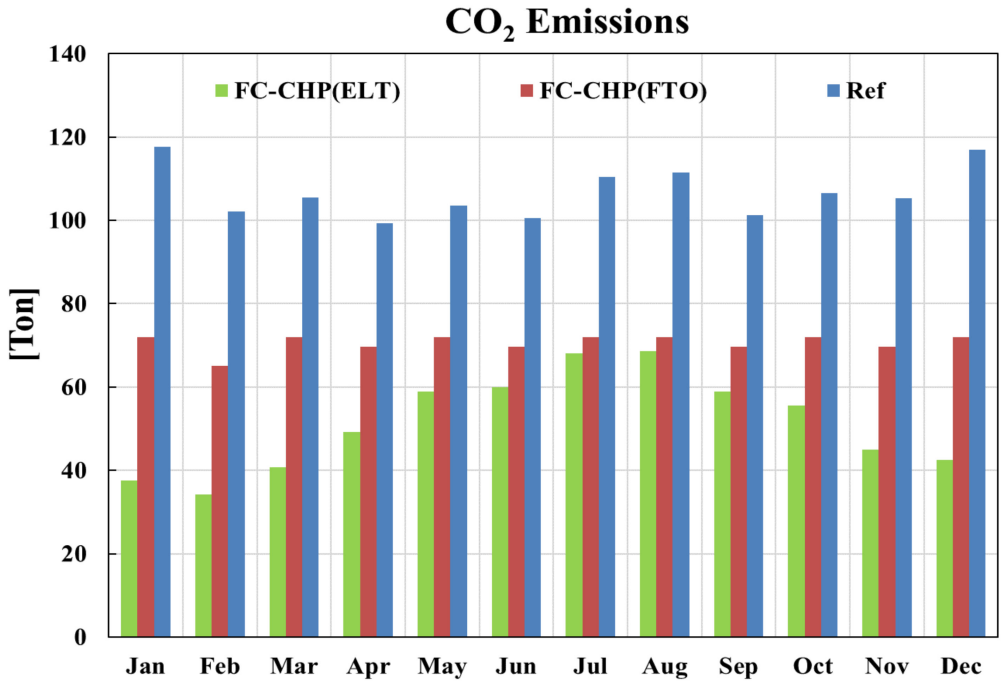

Figure 12. CO_2 emissions for the three case studies (ELT and FTO models in FC-CHP systems and the conventional energy supply model).

The fuel cell efficiency was defined in Equations (1)–(3). The fuel cell is supported to operate with a maximum capacity for all of the time under the FTO operating model so that it can give a significantly high efficiency than the ELT model which is operating by following the electricity load. Here, it has to be mentioned that, for the investigation of the fuel cell efficiency, only the total generation of power and heat are considered. Figure 13 shows the total efficiency of the fuel cell under both operating models. By considering the utilization of energy, the efficiency of the FC-CHP system can be evaluated as follows:

$$\eta_{FC-CHP} = (E_{FC} + Q_{FC-B})/F_{FC} \quad (15)$$

where the E_{FC} is the electrical power generation from the fuel cell, $Q_{FC\text{-}B}$ is the recovered heat from the fuel cell and supply to the building, and F_{FC} is the fuel (natural gas) energy consumption of the fuel cell. Here, the electric power generation for the FTO model includes both amounts which will be supplied to the building and sold to the grid. From Figure 14, we can see that for both the FTO and ELT models, the FC-CHP system presents higher efficiency in winter (about 55% to 60%) than in summer (40% to 50%), because of the high heating demand in winter. From the point of view of the overall efficiency of the fuel cell system, the FTO model has a large advantage over the ELT model. However, at the same time, a large amount of heat generated under the FTO operating model cannot be supplied to the building, but is released to the ambient environment. This is why, when it comes to the system's efficiency, there is not much difference between the two models.

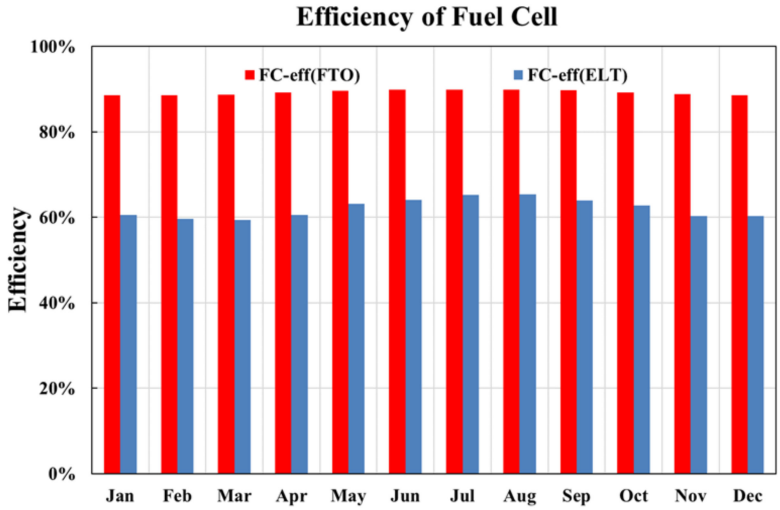

Figure 13. Total efficiency of the fuel cell under the FTO and ELT operating models.

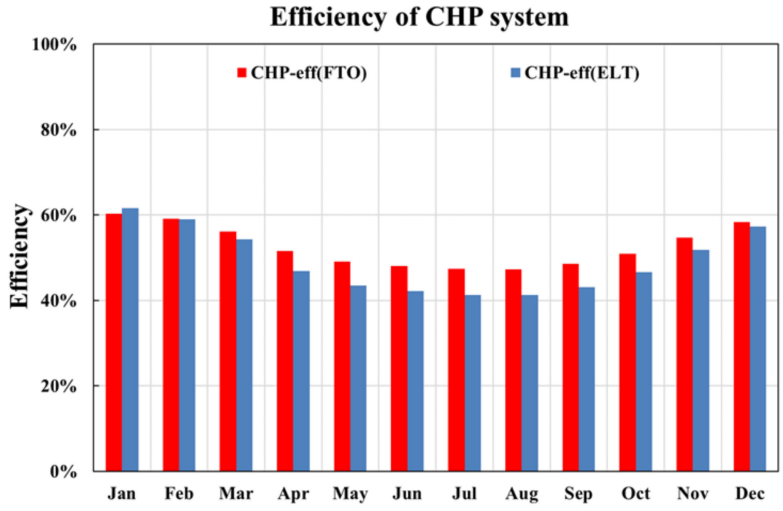

Figure 14. Efficiency of the FC-CHP system under the FTO and ELT operating models.

4. Economic Feasibility

From a general point of view, the fuel cell system is far from being economically feasible due to its high capital and operating cost [37]. However, a great potential has been presented for improving the utilization of energy productions, especially of thermal energy, due to the high heat demand of the commercial building in this study. The operating cost of the power and heat supply for the objective commercial building with an indoor swimming pool can be evaluated as:

$$C = C_f + C_{GE} - S_{EG} \tag{16}$$

where C_f is the cost of the fuel consumption of the fuel cell and boiler for both FC-CHP and conventional energy supply system. C_{GE} is the electric power cost from the main power grid, and S_{EG} is the income created by selling the excess electric power to the main power grid. The price of liquid natural gas (LNG) for industry and fuel cell applications is given as 44.98 and 44.13 USD/MWh (VAT included), respectively [38]. Unlike the price of natural gas, the selling price of fuel cell electricity to the grid is relatively unstable, and should be evaluated as:

$$p_{sell} = \text{SMP} + c_{FC}\text{REC} \tag{17}$$

In Korea, when selling electricity produced by fuel cell, the price is determined by the System Marginal Price (SMP) [39] and the unit price of Renewable Energy Certificates

(REC). REC certifies that power generators produced and supplied electricity by using new and renewable energy facilities, and the weighting factor of fuel cell (c_{FC}) application in Korea is given to be two [40]. Due to the fact that the SMP and the price of REC may fluctuate in real-time, which will have big impacts on the selling price of the electricity, a sensitivity analysis for the effect of the SMP and REC price was carried out by setting the selling price to low, medium and high levels. In Table 4, the monthly average value of the SMP and REC from January 2019 to present are evaluated and set to be the medium level of the price. The low and high level of the price are evaluated by raising and lowering the medium level price by 15%, respectively.

Table 4. SMP and REC prices.

	SMP (USD/MWh)	REC (USD/MWh)
Low (L)	60.24797	36.17903
Medium (M)	70.87996	42.56356
High (H)	81.51196	48.94809

Finlay, the net profit (NP) for the FC-CHP system compared with the conventional energy supply system is evaluated as:

$$\mathrm{NP} = C_{FC-CHP} - C_{REF} \tag{18}$$

The payback period (PP) is another important indicator for the evaluation of economic feasibility. Unlike a general economic model, the main benefit of applying the FC-CHP system is to obtain energy and cost saving by methods other than the traditional energy supply mode. Therefore, the payback period of the FC-CHP system could be simply evaluated by

$$\mathrm{PP} = C_0/(\mathrm{NP} - C_{MD}) \tag{19}$$

Here, C_0 and C_{MD} are the initial cost of the fuel cell system installation, and the maintenance and depreciation cost, respectively. The investment costs, including the fuel cell cost, installation cost, maintenance and depreciation costs are listed in Table 5. Here, it has to be mentioned that for both of the CHP and traditional system, the boiler and storage tank are needed. In this study, the cost saving by the reduction of the storage tank and boiler capacities are ignored.

Table 5. Investigation of the investment and incentive.

Total cost for fuel cell CHP system	$1,800,000
Installation cost	$600,000
Maintenance and depreciation costs	$50,000/year
Incentive from local government	$500,000
Total initial cost (with incentive)	$1,900,000
Total initial cost (without incentive)	$2,400,000

Table 6 summarizes the monthly operating cost and the net profit of the FC-CHP system under the ELT by comparing it with the conventional system. For the ELT model, the economic benefits are not significant. Even in March, April, May, September, and October, there is not only the profit but also the amount of loss presented. In the case of the FTO model, a sensitivity analysis for the economic feasibility is needed due to the large fluctuation of the SMP and REC prices. As shown in Table 4, the SMP and REC price are evaluated into low (L), medium (M) and high (H) levels. Thus, a total of nine market conditions of the electricity selling price are defined by the combination of the SMP and REC prices in different levels. For example, the condition of "LM" indicates that the

electricity selling price will be calculated with the low level of the SMP and the medium level of the REC price. Table 7 presents the monthly and annual operating costs of the FC-CHP system under the FTO model and the net profit (NP) by comparing them with the conventional energy supply system in MM condition. A significant net profit is obtained due to that the fuel cell operating for the full time within its rated capacity. A large amount of excess electricity could be sold to the grid. The annual net profit is about 226,097 USD in the MM condition.

Table 6. Operating cost of the FC-CHP model under the ELT operating model and the net profit (NP), in comparison with the conventional energy supply system.

Month	Caparison Data Sets of Operating Cost ($: USD)						
	New System with FC-CHP (ELT)			Reference Data from Conventional System			NP
	Fuel Cost	e-Cost	Total	Fuel Cost	e-Cost	Total	
Jan	23,835	2861	26,696	9446	25,103	34,549	7853
Feb	21,217	2572	23,789	8049	22,489	30,538	6748
Mar	22,363	1930	24,293	7504	17,832	25,337	1043
Apr	21,782	2212	23,994	5174	17,993	23,168	−827
May	22,888	2458	25,347	4156	18,886	23,042	−2305
Jun	22,280	3605	25,885	3544	26,995	30,540	4655
Jul	23,710	3449	4655	3344	28,338	31,682	27,026
Aug	23,695	4830	28,525	3295	28,419	31,714	3188
Sep	22,247	2434	24,680	3780	18,642	22,422	−2259
Oct	22,896	2401	25,297	5033	19,252	24,285	−1012
Nov	21,905	3006	24,911	6604	24,344	30,948	6037
Dec	23,214	3394	26,608	8548	25,641	34,189	7581
Sum	272,032	35,152	284,680	68,478	273,934	342,412	57,728

Table 7. Operating cost of the FC-CHP model under the FTO operating model and net profit (NP), in comparison with the conventional energy supply system.

Month	Caparison Data Sets of Operating Cost ($: USD)							
	New System with FC-CHP (FTO)				Reference Data from Conventional System			NP
	Fuel Cost	e-Cost	e-Sale	Total	Fuel Cost	e-Cost	Total	
Jan	35,432	843	26,948	9327	9446	25,103	34,549	25,222
Feb	32,004	849	25,275	7578	8049	22,489	30,538	22,960
Mar	35,432	810	29,030	7212	7504	17,832	25,337	18,125
Apr	34,289	1104	27,468	7925	5174	17,993	23,168	15,242
May	35,432	1268	27,105	9596	4156	18,886	23,042	13,447
Jun	34,289	1857	25,853	10,294	3544	26,995	30,540	20,246
Jul	35,432	2881	25,409	12,904	3344	28,338	31,682	18,777
Aug	35,432	2780	25,074	13,139	3295	28,419	31,714	18,575
Sep	34,289	1250	25,538	10,001	3780	18,642	22,422	12,421
Oct	35,432	1122	26,630	9925	5033	19,252	24,285	14,359
Nov	34,289	1291	26,899	8682	6604	24,344	30,948	22,267
Dec	35,432	1514	27,214	9733	8548	25,641	34,189	24,456
Sum	417,189	17,569	318,442	116,315	68,478	273,934	342,412	226,097

Figure 15 presents the net profits and payback period in nine price conditions when the system is operating with the FTO model. The net profit made in comparison with the conventional energy supply system is about 178,352 to 273,879 USD per year. As we investigated, the initial costs for a 440 kW PAFC base CHP system with and without incentives are around 1,900,000 and 2,400,000 USD, respectively. If the system is operating with the FTO model, the payback periods with and without incentives from the local government are 6.9 to 10.7 years and 8.8 to 13.5 years, respectively.

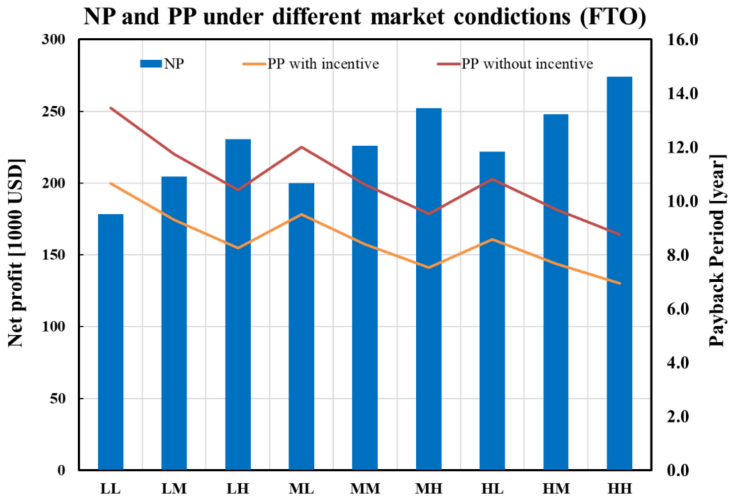

Figure 15. Net profit and payback period under the FTO model with different electricity market conditions.

5. Conclusions

In this study, a comprehensive sports center with an indoor swimming pool which is under construction in Donghae City, Korea is supported by a 440 kW PAFC-based CHP system for its electrical and thermal energy supply. The dynamic simulation of the energy supply system based on the investigated fuel cell performance data, the electrical load of a reference commercial building, and the evaluated thermal load was carried out for the cases with the ELT and FTO operating model. From the results, several key conclusions can be derived as follows:

1. A weather-data-based dynamic simulation model of the FC-CHP system including the components of the 3D-building load, fuel cell system, back-up boiler, heat exchanger, and storage tank was developed. The thermal load was obtained from the dynamic simulation, and was well-validated by the measured data. It can provide a reliable basis for the system simulation, thereby enhancing the credibility of the simulation results.
2. The FTO model was applied as one of the strategies for the fuel cell operating in a CHP system, and was simulated by the dynamic model and compared with the ELT model—which has been widely used in the CHP systems—and the conventional energy supply system in the aspects of primary energy consumption, fuel cell and system efficiency, and CO_2 emissions. From the simulation results, the FTO model presents the highest primary energy consumption and fuel cell efficiency, due to its long operating time and high capacity. The ELT model presents the lowest primary energy consumption, and can save 10% to 15% of the energy compared to the conventional energy system. However, the ELT model has a relatively low fuel cell efficiency compared to the FTO model. For both of FTO and ELT models, the FC-CHP system presents higher efficiency and CO_2 reduction.
3. In the analysis of the economic feasibility, the FTO model presents much better potential than the ELT model. The net profit made in comparison with the conventional energy supply system is about 178,352 to 273,879 USD per year, and the payback period is expected to be 6.9 to10.7 years under different market conditions.
4. Based on the analyses of the performance and economic feasibility of the system, the FTO model is suggested to be the operating strategy for the design of the fuel cell CHP system. However, more case studies with novel design parameters and operating strategies should be tested in future work.
5. As the objective building in this study is in construction now, the results obtained in this study should be validated by the real measured data after the system's completion.

More verification and testing will be helpful to improve the computational model, and thus make it more widely utilized.

Author Contributions: J.L., performed the system modeling and numerical analyses, and drafted the manuscript. S.-C.K., discussed the results. K.-Y.S., collected the measured data, organized the overall evaluation, and reviewed the manuscript. All authors have read and agreed to the published version of the manuscript.

Funding: This research received no external funding.

Institutional Review Board Statement: Not applicable.

Informed Consent Statement: Not applicable.

Data Availability Statement: Not applicable.

Acknowledgments: This work was funded by Donghae City, Gangwon Province, and supported by Donghae Coal-Fired Power Plant in Korea East-West Power Company and A1 Engineering, as a project partner. The authors really appreciate their support during this project.

Conflicts of Interest: The authors declare no conflict of interest.

Nomenclature

A	Area (mm^2)
AFC	Alkaline fuel cell
c	Impact factor of renewable energy
C	Cost ($USD)
CHP	Combined heat and power
CV-RMSE	Coefficient of variance of the root mean square error
E	Electric power, energy (kW, kWh)
F	Fuel energy consumption
FC-CHP	Fuel-cell-based combined heat and power
h	Convective heat transfer coefficient (W/mK);
h_{evp}	Evaporation heat (kJ/kg)
m_{evp}	Mass of evaporation water (kg/m^2h)
MBE	Mean bias error
MCFC	Molten carbonate fuel cell
NP	Net profit (USD/year)
p	Price (USD/kWh)
PAFC	Phosphoric acid fuel cell
PEMFC	Proton exchange membrane fuel cell
PP	Payback period (year)
Q	Heat (kW)
REC	Renewable energy certificates
S	Economic income
SMP	System marginal price (USD/MWh)
SOFC	Solid oxide fuel cell
T	Temperature (°C)
U	Conductive heat transfer coefficient (W/mK)
v	Indoor air speed (m/s)
x	Humidity radio (kg/kg)
Greek symbols	
ε	Emissivity
σ	Stefan–Boltzmann constant (W/m^2K^4)

Subscripts	
0	Initial
a	Air
b	Boiler
cel	Celling
cond	Conduction
conv	Convection
evp	Evaporation
EG	Electric power sold to the main power grid
f	Fuel
FC	Fuel cell
FC-B	Fuel cell to building
FC-CHP	Fuel-cell-based CHP system
GE	Electric power supplied from the main power grid
pw	Wall surfaces of the swimming pool
rad	Radiation
REF	Reference
S	Surface of the swimming pool
sw	Swimming pool water

References

1. Arsalis, A. A comprehensive review of fuel cell-based micro-combined-heat-and-power systems. *Renew. Sustain. Energy Rev.* **2019**, *105*, 391–414. [CrossRef]
2. Mago, P.J.; Smith, A.D. Evaluation of the potential emissions reductions from the use of CHP systems in different commercial buildings. *Build. Environ.* **2012**, *53*, 74–82. [CrossRef]
3. Ahmed, S.; Papadias, D.D.; Ahluwalia, R.K. Configuring a fuel cell based residential combined heat and power system. *J. Power Sources* **2013**, *242*, 884–894.
4. Chamra, L.M.; Mago, P.J. Micro-CHP power generation for residential and small commercial buildings (Ch. 2). In *Electric Power Research Trends*; Schmidt, M.C., Ed.; Nova Science Publisher, Inc.: New York, NY, USA, 2007.
5. Gandiglio, M.; Lanzini, A.; Santarelli, M.; Leone, P. Design and optimization of a proton exchange membrane fuel cell CHP system for residential use. *Energy Build.* **2014**, *69*, 381–393.
6. Löbberding, L.; Madlener, R. Techno-economic analysis of micro fuel cell cogeneration and storage in Germany. *Appl. Energy* **2019**, *235*, 1603–1613. [CrossRef]
7. Staffell, I.; Ingram, A. Life cycle assessment of an alkaline fuel cell CHP system. *Int. J. Hydrogen Energy* **2010**, *35*, 2491–2505. [CrossRef]
8. U.S. Department of Energy. Available online: https://www.energy.gov/sites/prod/files/2016/06/f32/fcto_fuel_cells_comparison_chart_apr2016.pdf (accessed on 15 March 2021).
9. Verhaert, I.; Mulder, G.; De Paepe, M. Evaluation of an alkaline fuel cell system as a micro-CHP. *Energy Conv. Manag.* **2016**, *126*, 424–445.
10. Wang, Y.; Chen, K.S.; Mishler, J.; Cho, S.C.; Adroher, X.C. A review of polymer electrolyte membrane fuel cells: Technology, applications, and needs on fundamental research. *Appl. Energy* **2011**, *88*, 981–1007. [CrossRef]
11. Kang, K.; Yoo, H.; Han, D.; Jo, A.; Lee, J.; Ju, H. Modeling and simulations of fuel cell systems for combined heat and power generation. *Int. J. Hydrogen Energy* **2016**, *41*, 8286–8295.
12. Chahartaghi, M.; Kharkeshi, B.A. Performance analysis of a combined cooling, heating and power system with PEM fuel cell as a prime mover. *Appl. Therm. Eng.* **2018**, *128*, 805–817.
13. Park, Y.J.; Min, G.; Hong, J. Comparative study of solid oxide fuel cell-combined heat and power system designs for optimal thermal integration. *Energy Conv. Manag.* **2019**, *182*, 351–368. [CrossRef]
14. Naimaster IV, E.J.; Sleiti, A.K. Potential of SOFC CHP systems for energy-efficient commercial buildings. *Energy Build.* **2013**, *61*, 153–160.
15. Sorace, M.; Gandiglio, M.; Santarelli, M. Modeling and techno-economic analysis of the integration of a FC based micro-CHP system for residential application with a heat pump. *Energy* **2017**, *120*, 262–275.
16. Napoli, R.; Gandiglio, M.; Lanzini, A.; Santarelli, M. Techno-economic analysis of PEMFC and SOFC micro-CHP fuel cell systems for the residential sector. *Energy Build.* **2015**, *103*, 131–146.
17. Zhang, H.; Lin, G.; Chen, J. Multi-objective optimisation analysis and load matching of a phosphoric acid fuel cell system. *Int. J. Hydrogen Energy* **2012**, *37*, 3438–3446. [CrossRef]
18. Wu, M.; Zhang, H.; Zhao, J.; Wang, F.; Yuan, J. Performance analyzes of an integrated phosphoric acid fuel cell and thermoelectric device system for power and cooling cogeneration. *Int. J. Refrig.* **2018**, *89*, 61–69. [CrossRef]
19. Sammes, N.; Bove, R.; Stahl, K. Phosphoric acid fuel cells: Fundamentals and applications. *Curr. Opin. Solid State Mat. Sci.* **2004**, *8*, 372–378. [CrossRef]

20. Chen, X.; Wang, Y.; Cai, L.; Zhou, Y. Maximum power output and load matching of a phosphoric acid fuel cell-thermoelectric generator hybrid system. *J. Power Sources* **2015**, *294*, 430–436.
21. Ito, H. Economic and environmental assessment of phosphoric acid fuel cell-based combined heat and power system for an apartment complex. *Int. J. Hydrogen Energy* **2017**, *42*, 15449–15463. [CrossRef]
22. Acha, S.; Le Brun, N.; Damaskou, M.; Fubara, T.C.; Mulgundmath, V.; Markides, C.N.; Shah, N. Fuel cells as combined heat and power systems in commercial buildings: A case study in the food-retail sector. *Energy* **2020**, *206*, 118046. [CrossRef]
23. Mago, P.J.; Fumo, N.; Chamra, L.M. Performance analysis of CCHP and CHP systems operating following the thermal and electric load. *Int. J. Energy Res.* **2009**, *33*, 852–864. [CrossRef]
24. Im, Y.H.; Liu, J. Feasibility study on the low temperature district heating and cooling system with bi-lateral heat trades model. *Energy* **2018**, *153*, 988–999. [CrossRef]
25. Hawkes, A.D.; Leach, M.A. Cost-effective operating strategy for residential micro-combined heat and power. *Energy* **2007**, *32*, 711–723. [CrossRef]
26. Yan, H.L.; Wang, G.P.; Lu, Z.W.; Tan, P.; Kwan, T.H.; Xu, H.R.; Chen, B.; Ni, M.; Wu, Z. Techno-economic evaluation and technology roadmap of the MWe-scale SOFC-PEMFC hybrid fuel cell system for clean power generation. *J. Clean Prod.* **2020**, *255*, 120225. [CrossRef]
27. Al-Khori, K.; Bicer, Y.; Aslam, M.I.; Koç, M. Flare emission reduction utilizing solid oxide fuel cells at a natural gas processing plant. *Energy Rep.* **2021**, 5627–5638. [CrossRef]
28. Doosan Fuel Cell. Available online: https://www.doosanfuelcell.com/en (accessed on 21 May 2021).
29. Thomas Auer, Assessment of an Indoor or Outdoor Swimming Pool, TRNSYS-TYPE 144. Available online: https://sel.me.wisc.edu/trnsys/components/type144-manual.pdf (accessed on 20 March 2021).
30. Smith, C.C.; Lof, G.O.G.; Jones, R.W. Rates of evaporation from swimming pools in active use. *ASHRAR Trsns* **1998**, *104*, 14–23.
31. Lam, J.C.; Chan, W.W. Life cycle energy cost analysis of heat pump application for hotel swimming pools. *Energy Conv. Manag.* **2001**, *42*, 1299–1306. [CrossRef]
32. Liu, J.; Chunga, D.H.; Chung, M.; Im, Y.H. Development of load models and operation simulator for a building complex with mixtures of multi-type engines and renewable devices. *Energy Build.* **2018**, *158*, 831–847. [CrossRef]
33. Djunaedy, E.; Van Den Wymelenberg, K. Targeted Calibration of Energy Models for Existing Building. In Proceedings of the ASHRAE 2014 Conference, Seattle, WA, USA, 28 June–2 July 2014.
34. IEA (2021). Available online: https://www.iea.org/countries/korea (accessed on 30 May 2021).
35. Hong, J.H.; Kim, J.; Son, W.; Shin, H.; Kim, N.; Lee, W.K.; Kim, J. Long-term energy strategy scenarios for South Korea: Transition to a sustainable energy system. *Energy Policy* **2019**, *127*, 425–473. [CrossRef]
36. Nam, H.; Nam, H.; Lee, D. Potential of hydrogen replacement in natural-gas-powered fuel cells in Busan, South Korea based on the 2050 clean energy Master Plan of Busan Metropolitan City. *Energy* **2021**, *221*, 119783. [CrossRef]
37. Sevencan, S.; Lindbergh, G.; Lagergren, C.; Alvfors, P. Economic feasibility study of a fuel cell-based combined cooling, heating and power system for a data center. *Energy Build.* **2016**, *111*, 218–223. [CrossRef]
38. Korea City Gas Association. Available online: http://www.citygas.or.kr/index.jsp (accessed on 25 June 2021).
39. Ministry of Trade, Industry and Energy. Available online: http://english.motie.go.kr/www/main.do (accessed on 30 September 2021).
40. Korea Energy Agency. Available online: https://dco.energy.or.kr/renew_eng/main/main.aspx (accessed on 30 September 2021).